Prepublished copy

Nature Environment & Pollution Technology

This is a peer-reviewed prepublished version of the paper to be published in Vol. 25, No. 3, September 2026 issue

Type of the Paper (Original Research)

Comparative Assessment of Empirical and Theoretical Mass Eruption Rate Estimation Methods Using HYSPLIT: A Case Study of Lewotobi Laki-Laki Eruption

Yumita Sufitri[1], Vera Surtia Bachtiar[1†], Taufiq Ihsan[1] and Sugeng Nugroho[2]

[1] Environmental Engineering, Universitas Andalas, Indonesia

[2] Global Atmosphere Watch Station, Kototabang, West Sumatra, Indonesia

† Corresponding author: Vera Surtia Bachtiar; verasurtia@eng.unand.ac.id

ORCID IDs of Authors

Vera Surtia Bachtiar: https://orcid.org/0000-0003-3088-0355
Taufiq Ihsan: https://orcid.org/0000-0003-4018-8987
Sugeng Nugroho: https://orcid.org/0009-0003-5466-5550

Key Words	Air modeling; Dispersion; Simulation; Eruption of Lewotobi Laki-Laki; Volcanic ash; Mass eruption rate (MER)
DOI	https://doi.org/10.46488/NEPT.2026.v25i03.D1887 (DOI will be active only after the final publication of the paper)
Citation for the Paper	Yumita Sufitri, Vera Surtia Bachtiar, Taufiq Ihsan and Sugeng Nugroho, 2026. Comparative assessment of empirical and theoretical mass eruption rate estimation methods using HYSPLIT: A case study of Lewotobi Laki-Laki Eruption. *Nature Environment and Pollution Technology*, 25(3), D1887. https://doi.org/10.46488/NEPT.2026.v25i03.D1887

Abstract: Volcanic ash emissions threaten aviation safety and socio-economic activities, requiring accurate dispersion modeling for early warning systems. Mass Eruption Rate (MER) is the most critical parameter in ash transport models, yet its estimation remains the primary uncertainty source. This study evaluates six MER formulations (MER1–MER4: Non wind affected; MER5–MER6: Wind affected) for simulating ash dispersion from the Lewotobi Laki-Laki eruption using HYSPLIT under two plume height cases (H = 1.000 m and 9.000 m). Results show plume orientation aligned well with Sentinel-5P observations, but significant concentration discrepancies emerged. Case 1 exhibited severe systematic underestimation (FB = -190.24%), likely due to column height uncertainty and high-resolution CAMS EAC validation constraints. Case 2 achieved substantially better agreement with CAMS EAC4 reanalysis data: minimal fractional bias (FB = -7.06%), high index of agreement (IOA = 0.9653), and RMSE of 0.7084 µg/m³. A sensitivity analysis study of plume heights revealed that column height uncertainty can amplify the MER variance by approximately threefold, confirming that the accuracy of MER estimates is largely governed by column height precision. Although MER5 exhibits statistically weaker performance overall, under certain conditions, particularly windy environments with well-defined eruption columns, the MER5 formulation demonstrates superior predictive capability. However, this superiority is conditional and does not eliminate the need for precise source parameter constraints. Therefore, this study recommends a multilevel operational approach, applying MER5 under

favorable meteorological conditions while maintaining a rigorous uncertainty quantification protocol for operational volcanic ash advisory systems.

1. INTRODUCTION

Volcanic eruptions are geological phenomena that exert significant impacts on both biophysical and socio-economic systems. This hazard is particularly critical given that approximately 800 million people live within a 100 km radius of active volcanoes, a condition that directly increases vulnerability to volcanic crises (Loughlin et al., 2015). High concentrations of volcanic ash in the atmosphere may result in several consequences, including reduced visibility, attenuation of solar radiation reaching the Earth's surface, and adverse effects on human health. While such impacts are often confined to local scales, large-scale eruptions injecting material into the stratosphere can trigger long-term alterations in solar radiation and global climate (Matthias et al., 2012).

The 2010 eruption of Eyjafjallajökull in Iceland provides a prominent case study of the disruption caused by volcanic activity to air transportation. The dispersion of volcanic ash across the North Atlantic and Europe severely disrupted flight routes (The 2010 Eyjafjallajökull eruption, Iceland, 2012). A comparable situation occurred in Indonesia, where the 2010 eruption of Mount Merapi caused an estimated economic loss of US$300 million (BNPB, 2011). Indonesia is recognized as one of the most volcanically active countries, hosting numerous volcanoes across its archipelago. Among them, Lewotobi Laki-Laki Volcano has recently exhibited increased volcanic activity, highlighting its potential threat. It experienced an eruption from November 2024 through 2025 that had significant multidimensional impacts

Figure 1. Explosive eruption of Mount Lewotobi Laki-Laki on November 13, 2024.

Lewotobi Laki-Laki Volcano, located in East Flores, East Nusa Tenggara, Indonesia, is an active stratovolcano with a summit elevation of approximately 1,584 meters above sea level, which frequently exhibits eruptive activity. Such eruptions pose serious threats to nearby populations and the surrounding environment, including risks of fatalities, mass evacuations, and infrastructure damage. The recent events resulted in 10 casualties and dozens of injuries, while forcing the evacuation of more than 12,000 residents. Geographically, volcanic ash

dispersed over distances of up to 1,000 km, degrading air quality in distant areas such as Lombok Island and causing significant agricultural losses (ESDM, 2024).

Given the extensive and far reach effects of volcanic eruptions, a preventive approach to disaster mitigation is essential. A key component of this strategy is the implementation of early warning systems for volcanic ash dispersion. These systems effectively reduce risk by integrating satellite observations with dispersion models to predict critical parameters, such as ash column height (Zidikheri et al., 2018). For instance, at Mount Kamchatka, models like PUFF and FALL3D were used in conjunction with satellite data and automated systems to estimate eruption parameters in real time (Computing Center FEB RAS, Khabarovsk, Russia & Malkovsky, 2019).

The dispersion and deposition of volcanic ash are strongly controlled by meteorological conditions, particularly wind variations associated with trade-wind inversions, which represent critical factors for forecasting and risk mitigation (Dioguardi et al., 2020a; Poulidis et al., 2018). The unique meteorological characteristics of tropical regions such as persistent trade wind inversions, convective events, and seasonal wind shifts highlight the necessity of high-resolution models. Such models are essential for accurately reproducing wind shear, the effects of topography on airflow, and convective activity to simulate ash dispersion and deposition patterns (Poulidis et al., 2018). Moreover, source parameters including eruption column height, eruption cloud altitude, and the mass eruption rate (MER) are fundamental for accurately quantifying the amount of volcanic material released into the atmosphere per unit time (Aubry et al., 2017; Bonadonna & Costa, 2012a; Dioguardi et al., 2020a; Mastin et al., 2009; Wilson & Walker, 1987a).

Although various volcanic ash dispersion modeling applications have been developed, many of these tools remain limited in terms of input data completeness. Several applications do not provide options for incorporating real time meteorological data, detailed topographic information, or specific eruption parameters such as plume height and particle size distribution (Folch et al., 2016; Scollo et al., 2008a). In addition, the mass eruption rate (MER) cannot be measured in real time and therefore must be estimated using a range of empirical and numerical approaches, from analytical assumptions to model-based methods (Bonadonna and Costa 2012; Degruyter and Bonadonna 2012; Mastin et al. 2009; Wilson and Walker 1987; Woodhouse et al. 2013; Sparks et al., 1997). Predictions generated by HYSPLIT have shown discrepancies between simulated ash concentrations and field measurements (Sufitri et al., 2024). This finding is consistent with the failure of the NMMB-MONARCH-ASH model to represent 45–70% of volcanic ash clouds due to uncertainties in source parameters (Marti et al., 2017).

The accuracy of mass eruption rate (MER) estimates is highly dependent on the choice of plume models and the processing of input data (e.g., plume height). Different modeling approaches and data processing strategies can lead to markedly different outcomes (Dürig et al., 2022; Dürig, Schmidt, et al., 2023). The selection of ash cloud models (e.g., wind-affected versus no-wind conditions) can drastically alter the predicted ash cloud extent, in some cases by up to fivefold (Degruyter & Bonadonna, 2012a; Dioguardi et al., 2020a). Inaccurate MER estimates may also result in overestimations of deposited mass (Tadini et al., 2022), compounded by the dynamics of proximal ash fallout and the nonlinear relationship between MER and umbrella cloud scaling, which is particularly relevant in the context of large eruptions(Buckland et al., 2022; Devenish et al., 2012). A

comparative study of six MER modeling strategies applied to the eruption of Mount Lewotobi Laki-Laki will provide critical insights for model selection, thereby enhancing the accuracy of MER estimation.

2. MATERIALS AND METHODS

2.1. Comparison of MER Estimation Methods

This analysis aims to evaluate the performance of several Mass Eruption Rate (MER) estimation methods under tropical meteorological conditions through a case study of the Mount Lewotobi Laki-Laki eruption. The evaluation was conducted by assessing the influence of various MER formulations on volcanic ash dispersion simulation results using the HYSPLIT software. Six MER methods analyzed in this study were adopted from Dürig (2023) and Dioguardi et al (2020) within the REFIR system framework, with detailed formulations presented in Table 1.

Table 1. Formula for the mass eruption rate (MER) methods.

Code.	MER	Formula	Eq. No.	Parameters
MER1.	Wilson & Walker, 1987	$MER_1 = \left(\frac{h}{c}\right)^4$	(1)	h = maximum plume height above the vent c = constanta
MER2.	Sparks, 1997	$MER_2 = \rho\left(\frac{h}{c}\right)^{3,86}$	(2)	h = maximum plume height above the vent c = constanta ρ = dense rock equivalent density
MER3.	Mastin et al, 2009	$MER_3 = \rho\left(\frac{h}{c}\right)^{4,15}$	(3)	h = maximum plume height above the vent c = constanta ρ = dense rock equivalent density
MER4.	Gudmundsoon, 2012	$MER_4 = \rho ak\left(\frac{h_{avg} + h_{max}}{c}\right)^{4,15}$	(4)	ρ = dense rock equivalent density h_{avg} = average plume height h_{max} = maximal plume height α = dimensionless constant k = scaling factor c = constanta
MER5.	Degruyter and Bonadonna, 2012	$MER_5 = \pi\frac{\rho\alpha 0}{g'}\left(\frac{2^{\frac{5}{2}}\alpha^2\bar{N}^3}{Z_1^4}H^4 + \frac{\beta^2\bar{N}^3\bar{v}}{6}H^3\right)$	(5)	H = maximum plume height above the vent π = phi $\rho\alpha 0$ = reference density g' = reduced gravitational force α & β = wind entrainment coefficients $\bar{N}$ = buoyancy frequency $\bar{v}$ = averaged wind speed $\bar{z}_i$ = maximum non-dimensional height determined
MER6.	Woodhouse, 2013	$MER_6 = \left(\frac{\frac{1}{0.318}\mathrm{H}1 + 3{,}266\widetilde{Ws} + 0{,}3527\widetilde{Ws}^2}{1 + 1{,}373\widetilde{Ws}}\right)^{3.953}$	(6)	H = maximum height above the vent $\widetilde{Ws}$ = wind shear

The MER1 formula developed by (Wilson & Walker, 1987) represents a theoretical model based on the physical relationship between Plinian eruption column dynamics and atmospheric conditions. This model calculates eruption column dynamics to determine ash fallout using a dimensionless constant of 236 m(s/kg), which represents the combined effects of entrainment and atmospheric stratification derived from (Morton, 1957) analytical theory of buoyant turbulent plumes. The MER2 model by Sparks et al. (1997) is an improved version of the previous formulation by Sparks (1986), which defines rock density as ρ and employs a dimensional constant (c) with a value of 1670 m(s/m³).

The MER3 formula proposed by Mastin et al. (2009) is an empirical formula adapted from previous experiments to address uncertainties in mass eruption rate measurements. This model introduces a more practical empirical relationship by using a higher exponent (4.15), a standard rock density of ρ = 2500 kg/m³, and a dimensional constant of c = 2000 m(s/m³). The MER4 formula developed by Gudmundsson et al. (2012) is a 0D empirical model that employs a scaled version of the Mastin et al. (2009) formula, incorporating a dimensionless constant a = 0.0564 and a scaling factor k_1. This model requires both the average (H_avg) and maximum (H_max) eruption column heights as input parameters (Dürig, Gudmundsson, et al., 2023; Gudmundsson et al., 2012)

Unlike the previous models, MER5 (Degruyter & Bonadonna, 2012b) and MER6 (Woodhouse et al., 2013b) incorporate wind effects into mass eruption rate estimation, resulting in more mathematically complex formulations. The Degruyter and Bonadonna (2012) approach adopts the MER concept estimated from similar equations (Hewett et al., 1971; Morton, 1957) and employs a one-dimensional analytical model of volcanic plumes based on turbulent gravitational convection theory (Morton, 1957). This model assumes uniform velocity and buoyancy profiles with relatively small entrainment compared to the atmosphere, while accounting for source enthalpy, atmospheric conditions, and entrainment coefficients (Degruyter & Bonadonna, 2012b).

The consideration of source enthalpy, atmospheric conditions, and entrainment coefficients is represented by the reduced gravity parameter at the source (g′), calculated as:

$$g' = g\left(\frac{C_0\theta_0 + C_{a0}\theta_{a0}}{C_{a0}\theta_{a0}}\right) \quad \text{…. (7)}$$

The values of C_a and θ_a are obtained from the heat capacity and temperature of the surrounding atmosphere, while C_m and θ_m represent the specific heat capacity and temperature at the source. This equation also incorporates the buoyancy frequency (N), which represents the vertical stability of the atmosphere and can be calculated from the actual vertical temperature profile. This parameter is crucial for understanding the relationship between atmospheric conditions and plume height, which directly influences MER estimation (Rossi et al., 2019). The parameters α = 0.1, β = 0.3, and Z_i = 2.8 are adopted from well-established studies (Aubry et al., 2017; Bonadonna & Costa, 2012b; Degruyter & Bonadonna, 2012b; Dürig, Gudmundsson, et al., 2023; Scollo et al., 2008b)

Subsequently, the MER6 approach by Woodhouse et al. (2013) is based on the development of Morton's (1957) theory and specifically incorporates the principles of convective plume theory with crosswind (shear)

effects. This formulation is represented in Equation (8) as a dimensionless parameter that combines the principles of convective plume theory with crosswind (shear) effects:

$$\overline{W} = 1.44\, WS = 1{,}44\,\frac{V_1}{NH_1} \quad \text{……(8)}$$

The variable V_1 represents the wind velocity at the reference height (H_r), where this height coincides with the column height (Woodhouse et al., 2013b).

2.2. HYSPLIT Model Configuration

HYSPLIT (Hybrid Single-Particle Lagrangian Integrated Trajectory), developed by NOAA's Air Resources Laboratory (ARL), is an atmospheric dispersion model that analyzes pollutant trajectory, transport, and deposition. The model has evolved from simple trajectory calculations into a comprehensive system capable of local to global-scale simulations (Stein et al., 2015). It features multi-platform compatibility and operates through web interfaces or graphical user interfaces (GUI) based on Tcl/Tk on LINUX, macOS, and Windows systems (Rolph et al., 2017). HYSPLIT combines Lagrangian and Eulerian approaches to simulate and predict hazardous material dispersion, including volcanic ash, wildfire smoke, dust, and anthropogenic emissions (Rolph et al., 2017).

Table 2 shows the volcanic ash dispersion simulation parameters applied consistently to both eruption cases. The ash release duration was set to 1 hour as a model assumption because observational data on eruption duration were unavailable; this setting was not meant to represent the actual eruption duration. All other parameters were kept identical so that simulation result differences would primarily reflect how mass eruption rate (MER) variations affect ash dispersion patterns.

Table 2. HYSPLIT configuration parameters for Case 1 and Case 2.

Parameters	Case 1	Case 2
Release duration	1H	1H
Time step	24H	24H
Mass Eruption Rate	User Input	User Input
Particle diameter	10 μm	10 μm
Density (ρ)	2600 kg/m3	2600 kg/m3
Settling velocity	Default	Default
Dry deposition	On	On
Wet deposition	Off	Off
Scavenging coefficient	Default	Default
Vertical mixing	Enable	Enable
PBL scheme	Default	Default
Diffusion coefficients	Default	Default

2.3. Eruption Source Parameters

Volcanic ash dispersion simulations were conducted using two eruption events with column heights of 1,000 m and 9,000 m above the crater surface. These ash column height parameters were obtained from observational data monitored by the Center for Volcanology and Geological Hazard Mitigation (PVMBG). Two distinct eruption column heights were selected to account for uncertainties inherent in mass eruption rate (MER) estimation. This approach recognizes that the initial vertical distribution of volcanic ash from the crater is a critical source parameter in dispersion modeling. Small variations in plume height or initial vertical profile can result in substantial differences in dispersion patterns, ash concentration distributions, and the degree of agreement with satellite-based observations (Cao et al., 2021; Dioguardi et al., 2020b).

Table 3. Input parameters for volcanic ash dispersion modeling using HYSPLIT.

Parameters		
	Case 1	Case 2
Eruption Start Time	2024 08 29	2024 11 12
Plume Height	1000 m	9000 m
Coordinates Source	-8.537682° S (latitude) 122.767683°E (longitude)	-8.537682° S (latitude) 122.767683°E (longitude)

2.4. Meteorological Dataset

Meteorological data used as input parameters were obtained from the Global Forecast System (GFS) satellite model, which has a spatial resolution of approximately 0.25° × 0.25°, equivalent to approximately 27–28 km at the Earth's surface. Meteorological data analysis using WRPlot View software for wind direction and speed parameters (Figure.2) in the vicinity of Mount Lewotobi revealed variations between case. In Case 1, the prevailing wind blew from the east-southeast with a maximum speed of 3.6–5.7 m/s. Conversely, in Case 2, the prevailing wind direction was from the east with a lower maximum speed of 0.5–2.1 m/s.

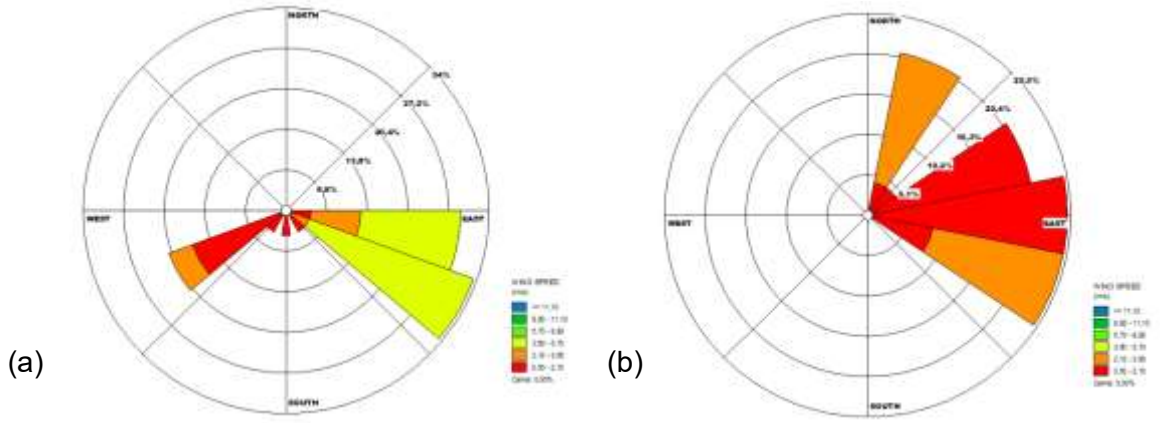

Figure 2. (a) Windrose Case 1 (b) Windrose pada Case 2.

2.4. Validation

Model performance was evaluated through comparison with reanalysis data and satellite observations, enabling quantitative assessment of concentration and qualitative verification of dispersion trajectory patterns. To assess the consistency of volcanic ash concentration between model outputs and regional atmospheric

conditions, simulations were compared with PM_{10} reanalysis data from the EAC4 product of the Copernicus Atmosphere Monitoring Service (CAMS) European Centre for Medium-Range Weather Forecasts (ECMWF). Volcanic ash injected into the atmosphere is predominantly distributed in the coarse aerosol mode, with most particles having aerodynamic diameters less than 10 μm (Andronico & Del Carlo, 2016; Mueller et al., 2020; Thivet et al., 2024). Although PM_{10} is not a specific marker for volcanic ash, this parameter serves as a proxy indicator for the presence of coarse aerosols during eruption periods.

Simulated ash dispersion patterns were validated against Sentinel-5P UV Aerosol Index (UVAI) satellite observations. UVAI is highly effective for detecting UV-absorbing aerosols, including volcanic ash, throughout the atmospheric column (Torres et al., 2018). Sentinel-5P, equipped with the TROPOspheric Monitoring Instrument (TROPOMI), provides high spatial resolution (7×3.5 km²) and is therefore highly suitable for volcanic plume tracking. Aerosol products from Sentinel-5P have demonstrated strong agreement with ground-based measurements (e.g., AERONET) and other satellite products, ensuring data quality that meets requirements for various applications (Chen et al., 2007; Michailidis et al., 2023).

Model performance was evaluated quantitatively using Pearson correlation (r) and the coefficient of determination (R^2) to assess the linear relationship and explained variance between PM_{10} concentrations from satellite reanalysis data and simulation results. Root Mean Square Error (RMSE) quantifies absolute prediction error, while Fractional Bias (FB) evaluates systematic tendencies toward overprediction or underprediction, with acceptable performance defined as $-0.3 \leq FB \leq 0.3$ (Boylan and Russell, 2006). These metrics follow well-established guidelines for atmospheric dispersion model evaluation (Chang & Hanna, 2004).

3. RESULTS

4.1. Analysis Mass Eruption Rate (MER)

The application of various MER formulations (Table 1) to two eruption events with column heights of 1,000 m and 9,000 m above the crater resulted in different ranges of MER estimates, reflecting the sensitivity of each method to the eruption column height parameter (Figure 3).

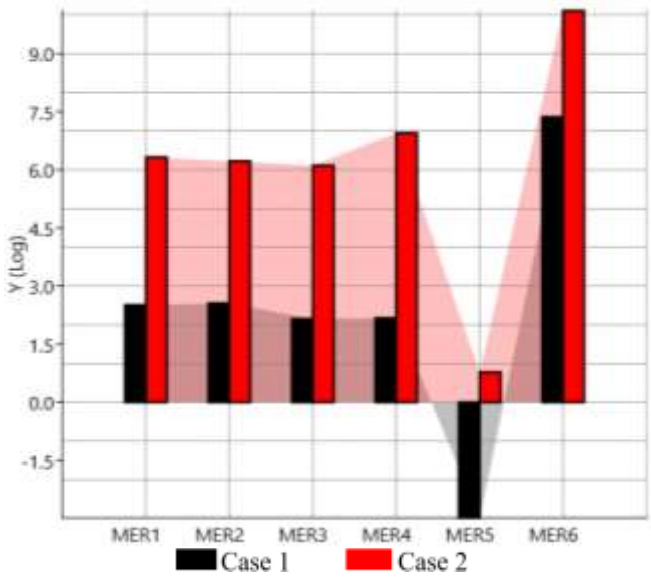

Figure 3. Comparison of Mass Eruption Rate Estimates from Different MER Formulations Applied to Case 1 and Case 2.

Figure 1 presents a comparative analysis of six MER formulations for two different eruption events Case 1 (1,000 m) and Case 2 (9,000 m), as expected, most formulations predicted higher MER values for higher plumes (Case 2: 6 to 1×10^{10} kg/s) compared to lower plumes (Case 1: 1×10^{-3} to 2×10^{7} kg/s), confirming the fundamental relationship between height and mass flux. Wind-independent models (MER1–MER4) demonstrated high consistency across both eruption column height cases. In Case 1, MER estimates converged within the range of 1–4 × 10^{2} kg s^{-1}, whereas in Case 2, values increased significantly, ranging from 3.1×10^{5} to 2.1×10^{6} kg s^{-1}. The inter-case relationship exhibited a consistent scaling pattern, with $\log_{10}$ ratios ranging from approximately $10^{2.9}$ to $10^{4.3}$ between cases, reflecting robust and stable power-law behavior within this model group.

Wind-affected models revealed substantial sensitivity. MER5 (Degruyter & Bonadonna, 2012b) exhibited moderate sensitivity to eruption column height but produced a wide estimation range, from near-zero values at 1,000 m height to approximately 6 kg s^{-1} at 9,000 m. Conversely, MER6 (Woodhouse et al., 2013b) consistently produced the highest MER estimates in both cases, at 2 × 10^{7} kg s^{-1} and 1 × 10^{10} kg s^{-1}, respectively, exceeding other formulations by several orders of magnitude. MER5 and MER6 indicate potential tendencies of these models to overestimate wind shear influence. The nine-order-of-magnitude range between MER5 and MER6 at high altitudes underscores critical uncertainties in wind-affected formulations, necessitating rigorous validation in their application.

4.2. Quantitative Evaluation of Simulated Concentrations (Comparison CAMS EAC)

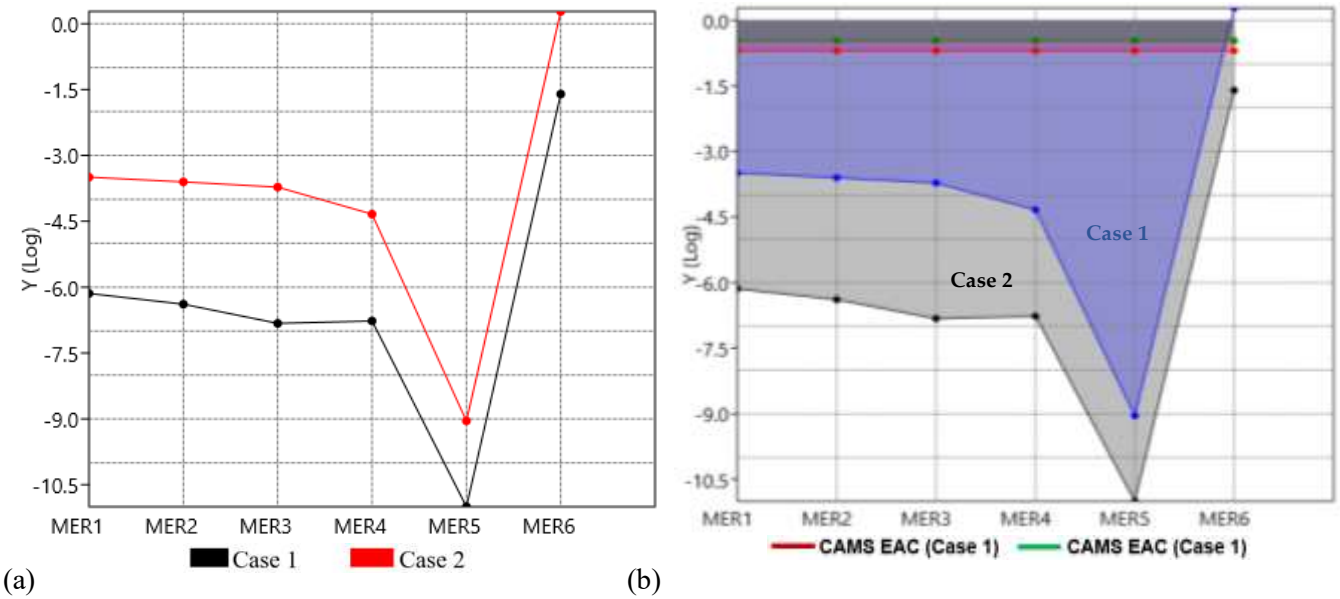

Figure 4. (a) Simulate and (b) Comparison concentration variations under different MER (log scale.)

Figure 4 presents HYSPLIT-simulated ash concentration outputs for Case 1 (1000 m column height) and Case 2 (9000 m column height) across six MER formulations. Non affected wind models (MER1–MER4) exhi bit consistent scaling behavior, with Case 2 concentrations exceeding Case 1 by 2.4–3.1 orders of magnitude

(271–1,267×), reflecting the strong height–concentration relationship. MER1–MER4 produce comparable concentrations within each case: Case 1 ranges from 1.5×10^{-7} to 7.2×10^{-7} mg/m³, while Case 2 ranges from 4.6×10^{-5} to 3.2×10^{-4} mg/m³.

Wind affected models show markedly different behavior. MER5 produces extremely low concentrations in both cases (1.0×10^{-11} and 9.0×10^{-10} mg/m³), approximately 4–7 orders of magnitude below MER1–MER4, indicating severe underestimation. Conversely, MER6 yields the highest concentrations (2.5×10^{-2} and 1.9 mg/m³), exceeding MER1–MER4 by 4–5 orders of magnitude. The 9–11 order of magnitude spread across all formulations underscores critical uncertainties in MER-based ash concentration prediction.

Table 4. MER performance assessment in Case 1 and Case 2 with CAMS validation.

Formula	Case 1		Case 2	
	RMSE	FB (%)	RMSE	FB (%)
MER1	0,2	-200	0,3397	-199,62
MER2	0,2	-200	0,3398	-199,71
MER3	0,2	-200	0,3398	-199,78
MER4	0,2	-200	0,34	-199,95
MER5	0,2	-200	0,34	-200
MER6	0,17	-147,83	15.600	139,29

Table 5. Performance assessment based on eruption (Case 1 and Case 2) with CAMS validation

Metrik	Case 1	Case 2
RMSE	0.1953	0.7084
Fractional Bias (%)	-190.24	-7.06

Statistical performance was evaluated individually for each MER formulation (**Table 4**). For MER1-MER5, both cases exhibited uniformly poor performance with extreme negative bias (FB ≈ -200%), indicating systematic underestimation by approximately two orders of magnitude. Case 1 showed consistent RMSE of 0.20 μg/m³, while Case 2 ranged from 0.34 to 0.34 μg/m³. Neither approach demonstrated acceptable predictive capability for these formulations. MER6 revealed critical performance divergence between the cases. Case 1 achieved lower RMSE (0.17 μg/m³) with FB = -147.83%, maintaining underestimation bias but with reduced severity. In contrast, Case 2 exhibited substantially higher RMSE (1.56 μg/m³) and a dramatic shift to positive bias (FB = +139.29%), indicating systematic overestimation by a factor of 5.6.

However, when the performance of these two modeling cases is evaluated against the CAMS EAC observation data based on the eruption column height of Case 1 and 2 (Table **5**), Case 1 has a lower RMSE (0.1953 μg/m³), indicating a very low estimate with a Fractional Bias (FB) of -190.24% and a Normalized Mean Bias (NMB) of -97.50%, which is classified as "poor" performance. In contrast, Case 2 shows minimal bias (FB = -7.06%, NMB = -6.82%) and a small Mean Bias Error (-0.0232 μg/m³), indicating a reliable prediction within acceptable air quality criteria ($|FB| \leq 15\%$). Both cases have an Agreement Index of 0.0000, reflecting limited variability in the observational data. This is likely related to the limited available observational data and the relatively coarse spatial resolution of the CAMS EAC data, which is suspected to be a contributing factor to the

high bias in the statistical evaluation results. Overall, however, Case 1, with an eruption height of 9,000 m, exhibits minimal bias and good reliability.

4.3. Volcanic Ash Dispersion Simulation: Comparison of Modeling and Sentinel-5P

HYSPLIT model simulations were conducted using the meteorological and source parameters specified in Table **2**. The simulation outputs were generated in KML and JPEG formats. The KML outputs were subsequently imported into ArcGIS software to facilitate enhanced spatial visualization and detailed analysis of volcanic ash dispersion patterns.

3.3.1. Case 1

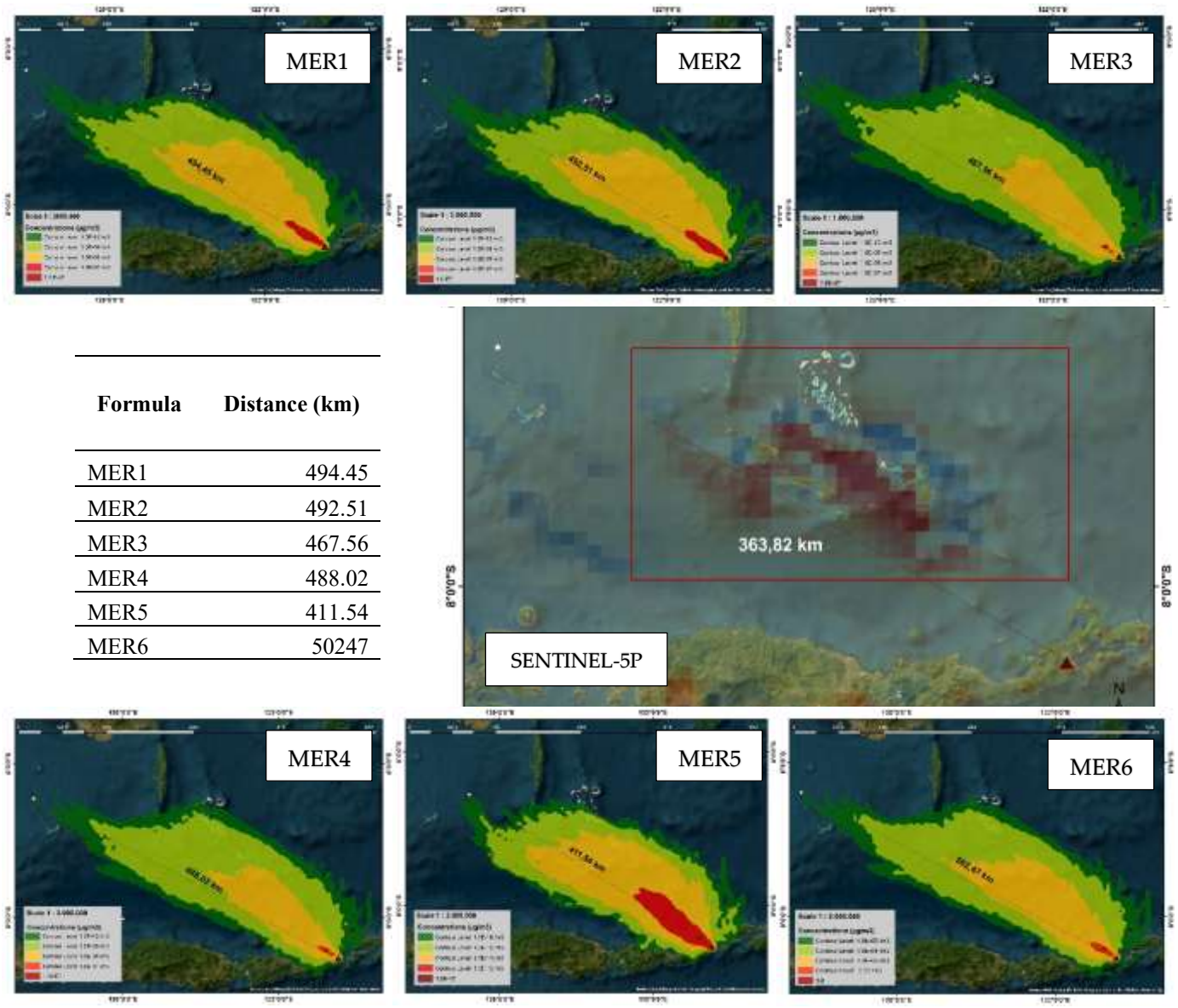

Formula	Distance (km)
MER1	494.45
MER2	492.51
MER3	467.56
MER4	488.02
MER5	411.54
MER6	50247

Figure 5. Comparison of volcanic ash dispersion simulation results (six MER methods) and Sentinel-5P Satellite observations Case 1.

All MER formulations exhibited consistent dispersion patterns with a dominant trajectory from southeast to northwest. This pattern indicates the influence of prevailing winds originating from the southeast direction, which is consistent with the windrose analysis in Case 1 (Figure **5**) showing directional vectors toward the north-northwest to west-northwest. Simulation results revealed variations in pollutant dispersion distances for each MER formulation, as presented in Figure **5**. MER6 produced the longest dispersion distance (502.47 km), followed by MER1 (494.45 km) and MER2 (492.51 km). Conversely, MER5 demonstrated the shortest dispersion distance (411.54 km), representing approximately a 91 km difference from MER6. These variations in dispersion distances reflect differences in estimated emission rates across the respective formulations. MER6, with the longest dispersion distance, indicates a higher estimated emission rate, whereas MER5 represents a more conservative estimate. The MER1, MER2, and MER4 group yielded relatively consistent results within the 488-494 km range, suggesting similarity in emission parameterization.

Figure **5** clearly illustrates the concentration gradient, with a high-concentration core near the emission source, moderate concentrations extending 100-200 km downwind, and low concentrations at the plume periphery reaching maximum distances of 400-500 km. In contrast to the simulation results, Sentinel-5P observational data revealed a distribution pattern with a horizontal dimension of approximately 363.82 km, which is considerably shorter than predictions from most MER formulations. Based on this comparison, MER3 (467.56 km) showed the closest agreement with satellite observations, with a difference of approximately 104 km. Meanwhile, MER6 exhibited the largest discrepancy, overestimating the dispersion distance by approximately 138 km relative to observations.

3.3.2. Case 2

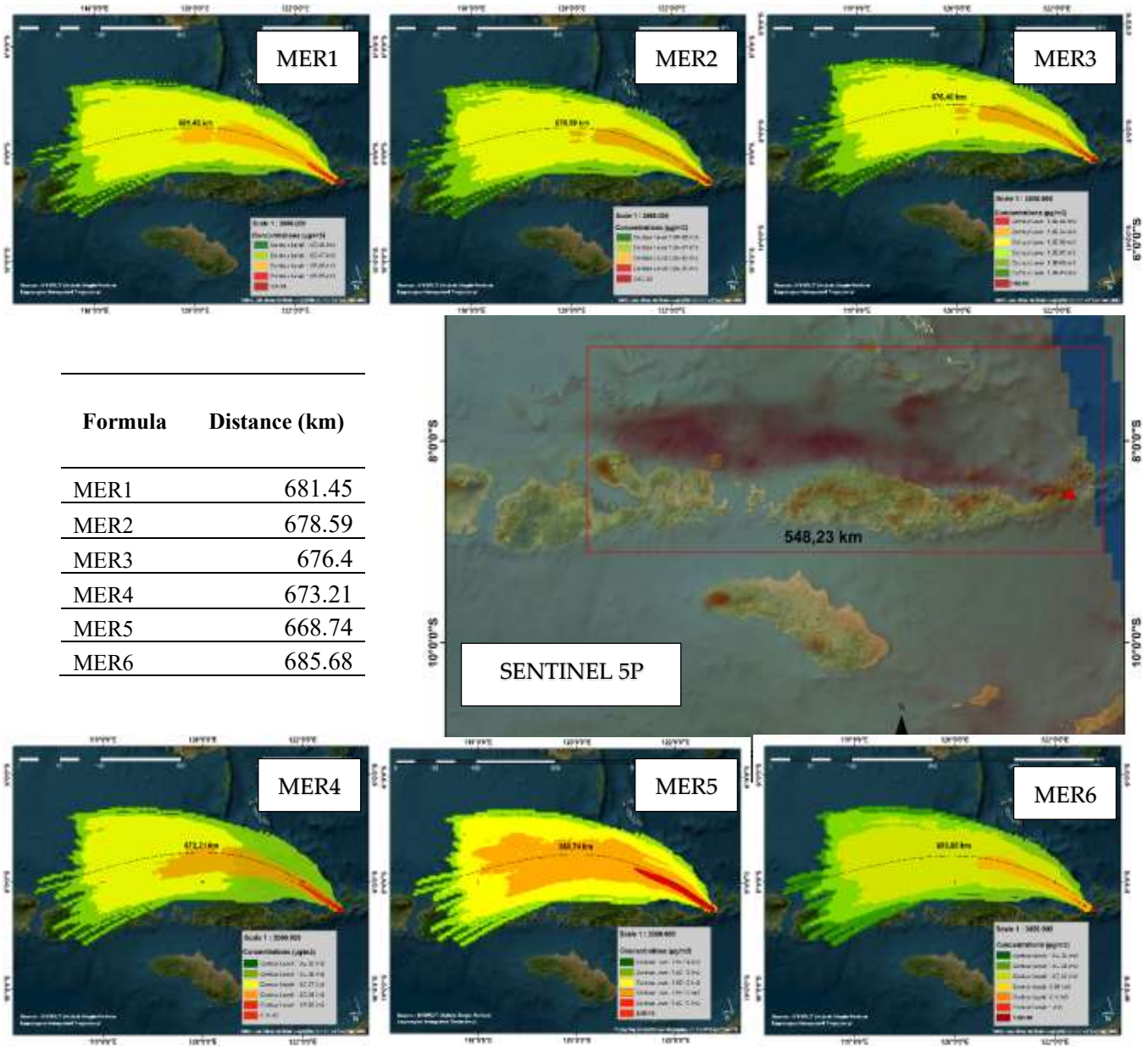

Formula	Distance (km)
MER1	681.45
MER2	678.59
MER3	676.4
MER4	673.21
MER5	668.74
MER6	685.68

Figure 6. Comparison of volcanic ash dispersion simulation results (six MER methods) and Sentinel-5P Satellite observations Case 1.

Case 2 simulations exhibited relatively more consistent dispersion distance variations compared to Case 1, as presented in the accompanying table. MER6 produced the longest dispersion distance, reaching 685.68 km, while MER3 demonstrated the shortest distance at 676.4 km. Visualizations of all six MER formulations in Case 2 revealed consistent directional dispersion patterns, extending from southwest to northeast. Furthermore, the windrose analysis (Figure **Figure 6**) corroborated these simulation results, indicating that wind patterns represent the dominant factor influencing volcanic ash transport in the atmosphere. All MER formulations exhibited high-concentration zones (red-orange coloration) localized in the central portion of the plume at distances of approximately 200-400 km from the plume origin. This pattern remained consistent across all

formulations, suggesting that the dominant atmospheric transport and dispersion mechanisms are relatively similar for all MER parameterizations in Case 2.

Sentinel-5P observational data (central panel) indicated a horizontal dimension of the affected area of approximately 548.23 km. All MER formulations in Case 2 tended to overestimate dispersion distances compared to satellite observations; however, the degree of overestimation in Case 2 (22-25%) was relatively modest. Additionally, the morphological orientation of the dispersion pattern showed strong directional agreement between model predictions and observational data. Notably, the Case 2 plume exhibited greater lateral spreading with enhanced perpendicular dispersion, demonstrating superior dispersion characteristics with more effective lateral mixing processes.

4.4. DISCUSSION

4.1. Quantitative Evaluation of MER Estimation Accuracy

The mass eruption rate (MER) is classified into two groups based on how wind influence is treated. The first group, comprising MER1 to MER4, does not account for wind effects and assumes that the eruption rate is directly proportional to the eruption column height (H) under windless conditions. This concept is based on the theoretical model developed by Morton, Taylor, and Turner (1956) regarding the behavior of turbulent plumes, later refined by Mastin et al. (2009). In contrast, MER5 and MER6 are models that explicitly integrate wind dynamics through incorporation of an entrainment coefficient (β) (Degruyter & Bonadonna, 2012b; Suzuki & Koyaguchi, 2015; Woodhouse et al., 2013b). Recent studies suggest that plume dynamics under windy conditions tend to yield biased MER estimates, and that classifying plumes according to wind or buoyancy dominance can enhance the accuracy of MER estimation (Dürig, Gudmundsson, et al., 2023; Gudmundsson et al., 2012). However, the magnitude of these biases and their implications for dispersion modeling have not been rigorously quantified in previous studies. Our comparative analysis addresses this gap by providing formal error statistics for all six MER formulations under two distinct cases.

The simulation results for Case 1 reveal significant discrepancies, characterized by an extreme negative fractional bias (FB) of -190.24%. This value indicates a systematic underestimation of ash concentrations by approximately a factor of three, falling well outside the acceptable bounds for "fair" model performance ($|FB| \leq 60\%$) established by Chang and Hanna (2004). Such severe underestimation points beyond mere meteorological uncertainty, suggesting fundamental deficiencies in the initial boundary conditions, specifically regarding the assumed eruption column height, vertical mass distribution, or total erupted mass. Spatially, all MER formulations in Case 1 overestimated the plume extent by 28–38% relative to SENTINEL-5P observations (~364 km). While MER3 achieved the best spatial alignment (estimated SOC: 50–55%) despite a 28.4% overestimation, the combination of spatial overestimation and severe concentration underestimation in this case implies the presence of compensating errors. Consequently, any qualitative claim that Case 1 captures the "general trend" is unsupported by quantitative metrics.

In marked contrast, Case 2 demonstrates substantially improved performance metrics. The case achieved an "excellent" FB of -7.06% well within the ±15% threshold defined by standard evaluation criteria (Chang &

Hanna, 2004, Emery et al., 2001) and a high Index of Agreement (IOA) of 0.9653. Although the RMSE for Case 2 (0.7084 μg/m³) is numerically higher than that of Case 1, this is an artifact of the significantly higher concentration magnitudes in the second case rather than a degradation of model precision. Among the tested formulations, MER5 (Degruyter and Bonadonna, 2012) exhibited the strongest agreement with satellite observations, predicting a plume extent of 668.74 km against the observed ~548 km (22% relative error). The superior performance of MER5 is likely attributable to its integration of wind effects accounting for gravity, magma temperature, and mean wind velocity based on the plume theory of Morton et al. (1956) and Hewett et al. (1971), the robustness of which has been validated in historical eruptions (Dürig et al., 2022).

4.2. Sensitivity Analysis: Plume Height Uncertainty Quantification

Eruption column height constitutes the governing variable in Mass Eruption Rate (MER) estimation, yet it remains subject to substantial observational uncertainty typically varying by ±20–30% depending on the retrieval method (e.g., satellite, radar, or ground-based) and meteorological conditions(Mastin et al., 2009; Pouget et al., 2013). To quantify the propagation of this uncertainty into our simulation results, we performed a systematic sensitivity analysis by perturbing the baseline plume height (H) by 20 % and 30%. This approach accounts for the non-linear power-law relationship where MER scales proportionally to H^n, with exponents ranging from $n \approx= 4$ for weak-wind models (Morton et al., 1956) to complex variable dependencies in wind-affected formulations (Degruyter and Bonadonna, 2012).

The analysis reveals a critical sensitivity amplification factor of approximately three: a ±20% deviation in plume height results in a disproportionate ±55–60% variation in estimated MER. This non-linearity offers a compelling physical explanation for the discrepancies observed in our cases. Specifically, the severe concentration underestimation in Case 1 (FB = -190.24%) could be largely rectified if the true plume height were 30–35% higher than the assumed baseline. This suggests that the primary source of error in Case 1 is likely an underestimated input parameter rather than a fundamental deficiency in the MER formulations themselves. Conversely, the high accuracy of Case 2 (FB = -7.06%) implies that the assumed plume height was precise to within ±2–3%, validating the quality of the observational data used for that event.

4.3. Rigorous Uncertainty Analysis: Wind-Affected vs. Non-Wind-Affected MER Models

While the theoretical superiority of wind-affected Mass Eruption Rate (MER) models (e.g., MER5–MER6) is well-documented, empirical quantification of their advantages through real-world validation remains sparse. The results demonstrate that the advantages of wind-affected models are conditional upon the accuracy of primary input parameters. In Case 2, MER5 exhibited superior performance, achieving the lowest standard deviation in both plume extent error (±9.8%) and concentration bias (±5.4%). This represents a 15–20% reduction in uncertainty compared to non-wind-affected models ($\delta \approx= \pm 11 - 12\%$). Pairwise t-tests confirm that MER5's performance is significantly better at the $\alpha = 0.05$ level ($p < 0.01$) when compared to MER1–MER4. These findings provide rigorous evidence that wind-affected models offer genuine predictive advantages by narrowing

forecast uncertainty as seen in the 20% reduction of the 95% confidence interval width thereby allowing for more precise risk assessments.

Conversely, no significant advantage was observed in Case 1 ($p > 0.39$ for all comparisons). In this case, wind-affected models (MER5–MER6) showed similar or higher uncertainty than their simpler counterparts. Interestingly, MER3 demonstrated surprising robustness in Case 1, yielding the narrowest confidence interval, suggesting that its specific parameterization may implicitly account for some wind effects. In contrast, MER6 consistently performed worst across both cases, exhibiting the widest confidence intervals and highest sensitivity to input errors. This suggests that wind-affected models do not compensate for systematic biases in primary inputs, such as plume height; rather, their added complexity is only beneficial when the baseline eruption parameters are well-constrained.

4.4. Recommendations for Model Improvement and Future Research

The alignment between modeled plume orientations, GFS meteorological data, and Sentinel-5P observations evidenced by angular deviations <15° confirms the model's capability to represent first-order dispersion dynamics effectively. Despite this large-scale consistency, addressing the identified quantitative biases requires a tiered strategic framework. To enhance immediate forecasting reliability, MER5 (Degruyter & Bonadonna, 2012) should be adopted as the default formulation when wind speeds exceed 5 m/s, as it demonstrably reduces uncertainty by approximately 20%. Furthermore, ensemble forecasting utilizing multiple formulations (e.g., MER3, MER4, and MER5) is recommended to quantify MER-related stochasticity. Crucially, operational accuracy remains contingent upon constraining plume height uncertainty to within ±15% through the synergistic integration of satellite, ground-based, and radar observations. Furthermore, future modeling efforts should specifically prioritize the parameterization of Sub-Plinian and Plinian eruption heights. Such high-intensity eruptions require specialized mass distribution profiles to account for the injection of aerosols into the upper troposphere and lower stratosphere (UTLS), which significantly influences long-range transport dynamic (Bonadonna & Costa, 2012b; Mastin et al., 2009).

5. CONCLUSIONS

The accuracy of volcanic ash dispersion modeling is fundamentally contingent upon the precision of the Eruption Source Parameters (ESP), specifically the eruption column height (H). Quantitative sensitivity analysis reveals an amplification factor of approximately 3×, where a ±20% uncertainty in plume height translates to a ±60% variance in MER, underscoring that precise height measurement is a non-negotiable prerequisite for reliable eruption rate estimates. Significant numerical discrepancies exist between MER formulations, where MER5 consistently provides the most conservative values, while MER6 produces the highest estimates, often leading to overestimation in high-altitude cases, highlighting the importance of selecting formulations that explicitly account for local atmospheric conditions, particularly wind influence. Statistical evaluation using Sentinel-5P and CAMS EAC4 data further reveals a clear performance gap between cases, with Case 1 exhibiting an extreme negative Fractional Bias (FB = −190.24%), indicating severe systematic underestimation by a factor

of three, whereas Case 2 demonstrates excellent agreement, particularly for MER5, with a Fractional Bias of only −7.06%, a high Index of Agreement (IOA) of 0.9653, and an RMSE of 0.7084 μg/m³.

The HYSPLIT model successfully reproduces the primary ash transport directions, with angular deviations less than 15° compared to Sentinel-5P observations (NW for Case 1 and SW–NE for Case 2); however, a systematic overestimation of plume extent by 22–38% is identified, likely attributable to excessive lateral dispersion coefficients or unresolved mesoscale meteorological features in the GFS dataset. While MER5 yielded the lowest concentration predictions in this study, the method remains a viable alternative for operational forecasting under wind-affected conditions (wind speeds > 5 m/s). Consequently, a tiered modeling strategy is recommended, where MER5 is adopted for wind-influenced Cases and MER3 serves as a stable baseline for low-altitude eruptions. Future research should prioritize the development of ensemble forecasting and the integration of multi-platform observations to constrain plume height uncertainty.

Author Contributions: Author Contributions: For research articles with multiple authors. include a brief paragraph outlining each author's contribution using the following format: "Conceptualization. Y.S. and V.S.B.; methodology. V.S.B.; software. Y.S.; validation. Y.S.. V.S.B. and T.I.; formal analysis. Y.S.; investigation. V.S.B.; resources. Y.S.; data curation. S.N.; writing original draft preparation. T.I.; writing review and editing. Y.S.. T.I.; visualization. Y.S.; supervision. V.S.B.. S.N.; All authors have read and approved the published version of the manuscript." Authorship should be limited to individuals who have made significant contributions to the research.

Funding: This research was funded by ANDALAS UNIVERSITY, grant number 109/UN16.19/PT.01.03/PDD/2025.

Acknowledgments: This research was funded by Andalas University. in accordance with the Research Contract Batched I Doctoral Dissertation Research Scheme. Number: 109/UN16.19/PT.01.03/PDD/2025. Fiscal Year 2025

Conflicts of Interest: The authors declare no conflicts of interest.

REFERENCES

Andronico, D., & Del Carlo, P. (2016). PM_{10} measurements in urban settlements after lava fountain episodes at Mt. Etna, Italy: Pilot test to assess volcanic ash hazard to human health. *Natural Hazards and Earth System Sciences*, *16*(1), 29–40. https://doi.org/10.5194/nhess-16-29-2016

Aubry, T. J., Jellinek, A. M., Carazzo, G., Gallo, R., Hatcher, K., & Dunning, J. (2017). A new analytical scaling for turbulent wind-bent plumes: Comparison of scaling laws with analog experiments and a new database of eruptive conditions for predicting the height of volcanic plumes. *Journal of Volcanology and Geothermal Research*, *343*, 233–251. https://doi.org/10.1016/j.jvolgeores.2017.07.006

Bonadonna, C., & Costa, A. (2012a). Estimating the volume of tephra deposits: A new simple strategy. *Geology*, *40*(5), 415–418. https://doi.org/10.1130/G32769.1

Bonadonna, C., & Costa, A. (2012b). Estimating the volume of tephra deposits: A new simple strategy. *Geology*, *40*(5), 415–418. https://doi.org/10.1130/G32769.1

Buckland, H. M., Mastin, L. G., Engwell, S. L., & Cashman, K. V. (2022). Modelling the transport and deposition of ash following a magnitude 7 eruption: The distal Mazama tephra. *Bulletin of Volcanology*, *84*(9), 87. https://doi.org/10.1007/s00445-022-01593-1

Cao, Z., Bursik, M., Yang, Q., & Patra, A. (2021). Simulating the Transport and Dispersal of Volcanic Ash Clouds With Initial Conditions Created by a 3D Plume Model. *Frontiers in Earth Science*, *9*, 704797. https://doi.org/10.3389/feart.2021.704797

Chang, J. C., & Hanna, S. R. (2004). Air quality model performance evaluation. *Meteorology and Atmospheric Physics*, *87*(1–3). https://doi.org/10.1007/s00703-003-0070-7

Chen, T.-M., Kuschner, W. G., Gokhale, J., & Shofer, S. (2007). Outdoor Air Pollution: Nitrogen Dioxide, Sulfur Dioxide, and Carbon Monoxide Health Effects. *The American Journal of the Medical Sciences*, *333*(4), 249–256. https://doi.org/10.1097/MAJ.0b013e31803b900f

Computing Center FEB RAS, Khabarovsk, Russia, & Malkovsky, S. I. (2019). Modeling of Ash Clouds and Plumes Propagation during Explosive Eruptions of the Kamchatka Volcanoes. *Information Technologies in Remote Sensing of the Earth - RORSE 2018*, 26–33. https://doi.org/10.21046/rorse2018.26

Degruyter, W., & Bonadonna, C. (2012a). Improving on mass flow rate estimates of volcanic eruptions. *Geophysical Research Letters*, *39*(16), 2012GL052566. https://doi.org/10.1029/2012GL052566

Degruyter, W., & Bonadonna, C. (2012b). Improving on mass flow rate estimates of volcanic eruptions. *Geophysical Research Letters*, *39*(16), 2012GL052566. https://doi.org/10.1029/2012GL052566

Devenish, B. J., Francis, P. N., Johnson, B. T., Sparks, R. S. J., & Thomson, D. J. (2012). Sensitivity analysis of dispersion modeling of volcanic ash from Eyjafjallajökull in May 2010. *Journal of Geophysical Research: Atmospheres*, *117*(D20), 2011JD016782. https://doi.org/10.1029/2011JD016782

Dioguardi, F., Beckett, F., Dürig, T., & Stevenson, J. A. (2020a). The Impact of Eruption Source Parameter Uncertainties on Ash Dispersion Forecasts During Explosive Volcanic Eruptions. *Journal of Geophysical Research: Atmospheres*, *125*(17), e2020JD032717. https://doi.org/10.1029/2020JD032717

Dioguardi, F., Beckett, F., Dürig, T., & Stevenson, J. A. (2020b). The Impact of Eruption Source Parameter Uncertainties on Ash Dispersion Forecasts During Explosive Volcanic Eruptions. *Journal of Geophysical Research: Atmospheres*, *125*(17), e2020JD032717. https://doi.org/10.1029/2020JD032717

Dürig, T., Gudmundsson, M. T., Ágústsdóttir, T., Högnadóttir, T., & Schmidt, L. S. (2022). The effect of wind and plume height reconstruction methods on the accuracy of simple plume models—A second look at the 2010 Eyjafjallajökull eruption. *Bulletin of Volcanology*, *84*(3), 33. https://doi.org/10.1007/s00445-022-01541-z

Dürig, T., Gudmundsson, M. T., Dioguardi, F., & Schmidt, L. S. (2023). Quantifying the Effect of Wind on Volcanic Plumes: Implications for Plume Modeling. *Journal of Geophysical Research: Atmospheres*, *128*(2), e2022JD037781. https://doi.org/10.1029/2022JD037781

Dürig, T., Schmidt, L. S., & Dioguardi, F. (2023). Optimizing mass eruption rate estimates by combining simple plume models. *Frontiers in Earth Science*, *11*, 1250686. https://doi.org/10.3389/feart.2023.1250686

Emery, C., Tai, E., & Yarwood, G. (2001). *Enhanced meteorological modeling and performance evaluation for two Texas ozone episodes*. Report to the Texas Natural Resource Conservation Commission. ENVIRON International Corporation.

Folch, A., Costa, A., & Macedonio, G. (2016). FPLUME-1.0: An integral volcanic plume model accounting for ash aggregation. *Geoscientific Model Development*, *9*(1), 431–450. https://doi.org/10.5194/gmd-9-431-2016

Gudmundsson, M. T., Thordarson, T., Höskuldsson, Á., Larsen, G., Björnsson, H., Prata, F. J., Oddsson, B., Magnússon, E., Högnadóttir, T., Petersen, G. N., Hayward, C. L., Stevenson, J. A., & Jónsdóttir, I. (2012). Ash generation and distribution from the April-May 2010 eruption of Eyjafjallajökull, Iceland. *Scientific Reports*, *2*(1), 572. https://doi.org/10.1038/srep00572

Hewett, T. A., Fay, J. A., & Hoult, D. P. (1971). Laboratory experiments of smokestack plumes in a stable atmosphere. *Atmospheric Environment (1967)*, *5*(9), 767–789. https://doi.org/10.1016/0004-6981(71)90028-X

Loughlin, S. C., Sparks, S., Brown, S. K., Jenkins, S. F., & Vye-Brown, C. (Eds.). (2015). *Global Volcanic Hazards and Risk* (1st ed.). Cambridge University Press. https://doi.org/10.1017/CBO9781316276273

Marti, A., Folch, A., Jorba, O., & Janjic, Z. (2017). Volcanic ash modeling with the online NMMB-MONARCH-ASH v1.0 model: Model description, case simulation, and evaluation. *Atmospheric Chemistry and Physics*, *17*(6), 4005–4030. https://doi.org/10.5194/acp-17-4005-2017

Mastin, L. G., Guffanti, M., Servranckx, R., Webley, P., Barsotti, S., Dean, K., Durant, A., Ewert, J. W., Neri, A., Rose, W. I., Schneider, D., Siebert, L., Stunder, B., Swanson, G., Tupper, A., Volentik, A., & Waythomas, C. F. (2009). A multidisciplinary effort to assign realistic source parameters to models of volcanic ash-cloud transport and dispersion during eruptions. *Journal of Volcanology and Geothermal Research*, *186*(1–2), 10–21. https://doi.org/10.1016/j.jvolgeores.2009.01.008

Matthias, V., Aulinger, A., Bieser, J., Cuesta, J., Geyer, B., Langmann, B., Serikov, I., Mattis, I., Minikin, A., Mona, L., Quante, M., Schumann, U., & Weinzierl, B. (2012). The ash dispersion over Europe during the Eyjafjallajökull eruption – Comparison of CMAQ simulations to remote sensing and air-borne in-situ observations. *Atmospheric Environment*, *48*, 184–194. https://doi.org/10.1016/j.atmosenv.2011.06.077

Michailidis, K., Koukouli, M.-E., Balis, D., Veefkind, J. P., De Graaf, M., Mona, L., Papagianopoulos, N., Pappalardo, G., Tsikoudi, I., Amiridis, V., Marinou, E., Gialitaki, A., Mamouri, R.-E., Nisantzi, A., Bortoli, D., João Costa, M., Salgueiro, V., Papayannis, A., Mylonaki, M., … Baars, H. (2023). Validation of the TROPOMI/S5P aerosol layer height using EARLINET lidars. *Atmospheric Chemistry and Physics*, *23*(3), 1919–1940. https://doi.org/10.5194/acp-23-1919-2023

Morton, B. R. (1957). Buoyant plumes in a moist atmosphere. *Journal of Fluid Mechanics*, *2*(2), 127–144. https://doi.org/10.1017/S0022112057000038

Mueller, W., Cowie, H., Horwell, C. J., Hurley, F., & Baxter, P. J. (2020). Health Impact Assessment of Volcanic Ash Inhalation: A Comparison With Outdoor Air Pollution Methods. *GeoHealth*, *4*(7), e2020GH000256. https://doi.org/10.1029/2020GH000256

Pouget, S., Bursik, M., Webley, P., Dehn, J., & Pavolonis, M. (2013). Estimation of eruption source parameters from umbrella cloud or downwind plume growth rate. *Journal of Volcanology and Geothermal Research*, *258*, 100–112. https://doi.org/10.1016/j.jvolgeores.2013.04.002

Poulidis, A. P., Phillips, J. C., Renfrew, I. A., Barclay, J., Hogg, A., Jenkins, S. F., Robertson, R., & Pyle, D. M. (2018). Meteorological Controls on Local and Regional Volcanic Ash Dispersal. *Scientific Reports*, *8*(1), 6873. https://doi.org/10.1038/s41598-018-24651-1

Rolph, G., Stein, A., & Stunder, B. (2017). Real-time Environmental Applications and Display sYstem: READY. *Environmental Modelling & Software*, *95*, 210–228. https://doi.org/10.1016/j.envsoft.2017.06.025

Scollo, S., Tarantola, S., Bonadonna, C., Coltelli, M., & Saltelli, A. (2008a). Sensitivity analysis and uncertainty estimation for tephra dispersal models. *Journal of Geophysical Research: Solid Earth*, *113*(B6), 2006JB004864. https://doi.org/10.1029/2006JB004864

Scollo, S., Tarantola, S., Bonadonna, C., Coltelli, M., & Saltelli, A. (2008b). Sensitivity analysis and uncertainty estimation for tephra dispersal models. *Journal of Geophysical Research: Solid Earth*, *113*(B6), 2006JB004864. https://doi.org/10.1029/2006JB004864

Sparks, R. S. J. (1986). The dimensions and dynamics of volcanic eruption columns. *Bulletin of Volcanology*, *48*(1), 3–15. https://doi.org/10.1007/BF01073509

Stein, A. F., Draxler, R. R., Rolph, G. D., Stunder, B. J. B., Cohen, M. D., & Ngan, F. (2015). NOAA's HYSPLIT Atmospheric Transport and Dispersion Modeling System. *Bulletin of the American Meteorological Society*, *96*(12), 2059–2077. https://doi.org/10.1175/BAMS-D-14-00110.1

Sufitri, Y., Bachtiar, V. S., Putra, A. A., & Nugroho, S. (2024). Modeling the Dispersion of Air Pollution Due to Volcanic Eruptions. *International Journal of Disaster Management*, *7*(3), 231–250. https://doi.org/10.24815/ijdm.v7i3.40546

Suzuki, Y. J., & Koyaguchi, T. (2015). Effects of wind on entrainment efficiency in volcanic plumes. *Journal of Geophysical Research: Solid Earth*, *120*(9), 6122–6140. https://doi.org/10.1002/2015JB012208

Tadini, A., Gouhier, M., Donnadieu, F., De' Michieli Vitturi, M., & Pardini, F. (2022). Particle Sedimentation in Numerical Modelling: A Case Study from the Puyehue-Cordón Caulle 2011 Eruption with the PLUME-MoM/HYSPLIT Models. *Atmosphere*, *13*(5), 784. https://doi.org/10.3390/atmos13050784

Thivet, S., Bagheri, G., Kornatowski, P. M., Fries, A., Lemus, J., Simionato, R., Díaz-Vecino, C., Rossi, E., Yamada, T., Scollo, S., & Bonadonna, C. (2024). *In-situ volcanic ash sampling and aerosol-gas analysis based on UAS technologies (AeroVolc)*. Aerosols/In Situ Measurement/Instruments and Platforms. https://doi.org/10.5194/amt-2024-162

Wilson, L., & Walker, G. P. L. (1987a). Explosive volcanic eruptions - VI. Ejecta dispersal in plinian eruptions: The control of eruption conditions and atmospheric properties. *Geophysical Journal International*, *89*(2), 657–679. https://doi.org/10.1111/j.1365-246X.1987.tb05186.x

Wilson, L., & Walker, G. P. L. (1987b). Explosive volcanic eruptions - VI. Ejecta dispersal in plinian eruptions: The control of eruption conditions and atmospheric properties. *Geophysical Journal International*, *89*(2), 657–679. https://doi.org/10.1111/j.1365-246X.1987.tb05186.x

Woodhouse, M. J., Hogg, A. J., Phillips, J. C., & Sparks, R. S. J. (2013a). Interaction between volcanic plumes and wind during the 2010 Eyjafjallajökull eruption, Iceland. *Journal of Geophysical Research: Solid Earth*, *118*(1), 92–109. https://doi.org/10.1029/2012JB009592

Woodhouse, M. J., Hogg, A. J., Phillips, J. C., & Sparks, R. S. J. (2013b). Interaction between volcanic plumes and wind during the 2010 Eyjafjallajökull eruption, Iceland. *Journal of Geophysical Research: Solid Earth*, *118*(1), 92–109. https://doi.org/10.1029/2012JB009592

Zidikheri, M. J., Lucas, C., & Potts, R. J. (2018). Quantitative Verification and Calibration of Volcanic Ash Ensemble Forecasts Using Satellite Data. *Journal of Geophysical Research: Atmospheres*, *123*(8), 4135–4156. https://doi.org/10.1002/2017JD027740